Investigation of trap states and mobility in organic semiconductor devices by dielectric spectroscopy: Oxygen-doped P3HT:PCBM solar cells

Oskar Armbruster,[1,*] Christoph Lungenschmied,[2,†] and Siegfried Bauer[1]
[1]*Department of Soft Matter Physics, Johannes Kepler University, Altenberger Straße 69, A-4040 Linz, Austria*
[2]*Konarka Austria F&E GmbH, Altenberger Straße 69, A-4040 Linz, Austria*
(Received 26 September 2012; published 3 December 2012)

We investigate the dielectric response of solar cell devices based on oxygen-doped poly(3-hexylthiophene):[6,6]-phenyl-C_{61}-butyric acid methyl ester (P3HT:PCBM) blends as a function of temperature between 133 K and 303 K. The spectra are analyzed using a recently introduced model [O. Armbruster, C. Lungenschmied, and S. Bauer, Phys. Rev. B **84**, 085208 (2011)] which is based on a trapping and reemission mechanism of charge carriers. A dominating trap depth of 130 meV is determined and the broadening of this trap level identified as purely thermal. In addition we estimate the density of charge carriers after doping as well as their mobility. We show that the concentration of mobile holes approximately doubles by heating the device from the lowest to the highest measured temperature. This is indicative of a second, shallow trap level of approximately 14 meV. Dielectric spectroscopy hence proves to be a valuable tool to assess device parameters such as dopant concentration, charge carrier transport characteristics, and mobility which are of crucial interest for understanding degradation in organic semiconductor devices.

DOI: 10.1103/PhysRevB.86.235201 PACS number(s): 68.55.Ln, 88.40.jr, 77.22.Gm, 73.50.Gr

I. INTRODUCTION

Organic solar cells have been shown to degrade upon exposure to atmosphere. The limited lifetime compared to their inorganic competitors is considered a major obstacle for widespread application and commercial success. In the following we demonstrate how dielectric spectroscopy can be used to elucidate phenomena such as doping, charge carrier trapping, and mobility in degraded organic photovoltaic (OPV) devices. We introduce a model which allows for the accurate description of their impedance spectra and the extraction of important device parameters by fitting to experimental data.

Despite the sensitivity of organic semiconductors, respectable lifetime results have been obtained, owing to the use of flexible barrier materials[2,3] or a favorable device architecture.[4] Alternatively, designing materials with improved intrinsic stability is highly promising. The challenge here is that oxygen, light, or water may not only interact with the absorber materials itself, but also with electrodes or interlayers and thereby negatively influence the device performance.[2,3,5,6] Studying the details of the predominant degradation mechanism in the photoactive layer under certain well-controlled conditions can be a first step to better understand and design more stable materials. Unfortunately degradation processes are not yet understood in sufficient detail in materials used for OPVs. Even for poly(3-hexylthiophene):[6,6]-phenyl-C_{61}-butyric acid methyl ester (P3HT:PCBM), probably the best-studied polymer:fullerene blend in OPVs to date, degradation mechanisms under various aging conditions require more attention. Details of the interaction of P3HT:PCBM thin-film devices with oxygen and light have been published recently. While these reports agree that a fundamental process is the doping of P3HT,[7–9] the consequences for charge transport and photovoltaic properties call for further investigation.

In this contribution, we report on dielectric spectroscopy data on P3HT:PCBM-based solar cells at various temperatures when degraded by exposure to oxygen and light. We attribute the features observed in the impedance spectra to charge transport in the presence of traps. Upon exposure to oxygen and light, mobile (positive) charges are introduced in the active layer of organic semiconductor devices.[5] Their ability to respond to an externally applied ac signal is limited by the presence of trap states which can capture the hole, immobilize it for a certain period of time, and eventually release it.[10] The average trapping time depends on the depth and capture cross-section of the trap and on the temperature of the hole. Figure 1 shows an illustration of the levels involved in charge transport and trapping. We identify two types of traps: deep traps 130 meV above the transport level and shallow traps with a depth of approximately 14 meV. The second type is within thermal energy at room temperature ($\approx$ 25 meV) and can hence more easily take part in charge transport compared to the deep-trap level. Applying an ac voltage to the two electrodes causes a periodic displacement of the mobile charges in the polymer.[11–13] The frequency of the ac voltage determines the average distance a hole can move in one half cycle. This movement of charges through the material is determined by the buildup of the electric field inside the device. It thus contributes to the out-of-phase current response (i.e., the capacitance) and is eventually limited by the width of the depletion region.

II. MODEL

In order to model the measured impedance data we describe our sample as a parallel-plate capacitor filled with a dielectric of a certain relative permittivity ($\underline{\varepsilon}$). Doping introduces additional holes in the active layer which causes the low-frequency capacitance to significantly exceed the geometric capacitance. In the presence of traps these charges may be immobilized for a certain time and only contribute to the capacitance when thermally reemitted. In order to account for this phenomenon we have previously introduced a Gaussian density of trap states (DOS) and assumed a Boltzmann term to describe the escape from the traps. In addition to this charge trapping

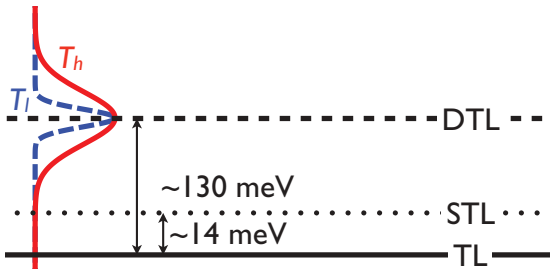

FIG. 1. (Color online) An illustration of the trap and transport levels as well as the thermal broadening of the deep trap level. TL: Transport level, STL: shallow trap level, DTL: deep trap level, T_l and T_h: density of trap states at low and high temperature.

effect, an accurate description of measured impedance spectra requires to account for an experimentally observed increase in capacitance with decreasing frequencies. A number of algorithms have been suggested to mathematically describe this phenomenon in a wide range of materials.[14,15] We have chosen an approach specifically introduced by Martens *et al.*[16] for conjugated polymer films intended to account for this dispersion of the relative permittivity of the active layer. A model which includes both these contributions in the representation of the real part of the dielectric permittivity is given by[1,17]

$$\varepsilon'_{\mathrm{DOS}}(f) = \frac{qd^2 N_{\mathrm{DOS}}}{2\varepsilon_0 U_{bi}} \left(1 - \mathrm{erf}\left[\frac{k_B T}{\sqrt{2}\sigma} \ln \frac{f}{f_0}\right]\right) + \underbrace{\frac{\varepsilon_\infty}{2} \frac{(2\pi f)^2 h}{g^2 + h^2}}_{\varepsilon_g}. \tag{1}$$

The detailed derivation of this dispersive DOS model is given in Ref. 1. Qualitatively, the error function (erf) in Eq. (1) introduces a transition between a plateau at high and one at low frequencies. This transition is centered around f_0 with its width given by σ. The height of the transition is determined by the charge density introduced due to doping (N_{DOS}) as well as the built-in potential (U_{bi}). The last term of Eq. (1), summarized as ε_g, accounts for the dispersive permittivity measured for the device excluding effects due to doping. ε_∞ represents the amplitude of the permittivity approached at high frequencies. Martens *et al.* originally introduced an M as a proportionality constant and γ as the dispersion coefficient in their model for the admittance of organic semiconductor devices.[16] We adopt this notation, but for clarity present the term using different parameters as defined in note 17. Parameter q denotes the charge of the electron, ε_0 the vacuum permittivity, d the active layer thickness, T the absolute temperature, k_B the Boltzmann constant, and f the frequency of the ac stimulus. The parameter in Eq. (1) which contains information about the characteristics of the dominating trap is f_0, the characteristic escape frequency. It denotes the inverse drift time a charge typically needs to travel across the depletion region and back. It is assumed that this movement is dominated by the time it takes charges to escape from these traps by thermal excitation. Hence an Arrhenius dependance between the depth of the trap and the characteristic escape frequency f_0 is implied as represented by Eq. (2), where ν denotes the attempt-to-escape frequency which includes information about the trapping cross-section.[11]

$$f_0(E) = \nu \exp\left[-\frac{E_0}{k_B T}\right]. \tag{2}$$

In Sec. IV, we present the results obtained by applying the DOS approach to dielectric spectra measured over a wide range of temperatures demonstrating the consistency between experimental data and the assumed Arrhenius dependance made in the derivation of the DOS model [Eq. (2)]. For this fitting procedure the free parameters are initially N_{DOS}/U_{bi}, f_0, σ to model the contribution of the dopants. ε_∞, M, and γ are the fit parameters used to describe the dispersive permittivity of the device.

A. Mobility

We assume that the characteristic escape frequency f_0 is the inverse time a hole needs to travel across the depletion region twice. Thus, $t_0 = 1/2f_0$ is the time necessary for the charge to drift under the influence of an electric field across the depletion region. For zero externally applied dc bias, this field is given by the built-in potential U_{bi}, resulting in a width W of the depletion zone of[7,18,19]

$$W = \sqrt{\frac{2\varepsilon_g \varepsilon_0 U_{bi}}{q N_{\mathrm{MS}}}}.$$

N_{MS} is the Mott-Schottky charge carrier concentration, which can be calculated from the charge carrier concentration N_{DOS} introduced in Eq. (1). There is a key difference between the two: In the derivation of the Mott-Schottky analysis, N_{MS} traditionally represents the total density of charge carriers within the volume formed by the depletion zone times the surface area of the electrodes. In Ref. 1, however, N_{DOS} is introduced in a way that it represents an average density of holes distributed across the whole volume of the active layer (i.e., the thickness of the active layer times the surface area of the electrode).

In the presence of a depletion zone, its width as well as the device area A determines the device capacitance C_{MS} at zero external dc bias.[7,18–21] The dimensionless relative permittivity $\varepsilon'_{\mathrm{MS}}$ can be calculated from C_{MS} and is given by

$$\varepsilon'_{\mathrm{MS}} = d\sqrt{\frac{q\varepsilon_g N_{\mathrm{MS}}}{2\varepsilon_0 U_{bi}}}. \tag{3}$$

The low-frequency limit $f \to 0$ (i.e., where the assumptions for Mott-Schottky are valid) of $\varepsilon'_{\mathrm{DOS}}$ taken from Eq. (1) is given by

$$\varepsilon'_{\mathrm{DOS}} = \frac{qd^2 N_{\mathrm{DOS}}}{\varepsilon_0 U_{bi}} + \varepsilon_g. \tag{4}$$

$\varepsilon'_{\mathrm{MS}}$ and $\varepsilon'_{\mathrm{DOS}}$ describe the same physical situation and hence have the same numerical value. One can thus combine Eqs. (3) and (4) and solve the resulting expression with regard to N_{MS}:

$$N_{\mathrm{MS}} = \frac{2U_{bi}}{q\varepsilon_g \varepsilon_0}\left(\frac{qdN_{\mathrm{DOS}}}{U_{bi}} + \frac{\varepsilon_g \varepsilon_0}{d}\right)^2.$$

At the characteristic escape frequency f_0, the voltage applied to the sample by the LCR meter is given by $U(t) = \hat{U}\sin(2\pi f_0 t)$. Hence, the electric field strength is given by

$E(t) = U(t)/W$. The drift velocity of a charge carrier in the electric field is defined as $v_d(t) = \mu E(t)$. It takes the charge carrier the time $t_0 = 1/2f_0$ to cover the distance W when traveling with velocity $v_d(t)$; thus the following relation holds:

$$W = \int_0^{t_0} dt\ v_d(t) = \frac{\mu \hat{U}}{W} \underbrace{\int_0^{t_0} dt\ \sin 2\pi f_0 t}_{(f_0\pi)^{-1}}.$$

Solving this equation to μ yields

$$\mu = \frac{W^2}{\hat{U}} f_0 \pi = \frac{\pi f_0 (\varepsilon_g \varepsilon_0 d)^2}{\hat{U}\left(d^2 q \frac{U_{bi}}{N_{\mathrm{DOS}}} + \varepsilon_g \varepsilon_0\right)^2}. \quad (5)$$

The mobility μ hence depends on N_{DOS}/U_{bi} which is an actual fit parameter in the dispersive DOS model [Eq. (1)]. Thus, no assumption (or measured value) of U_{bi} is necessary or will influence the quality of the results.

III. EXPERIMENTAL

In order to enable fast diffusion of oxygen into the active layer we chose P3HT:PCBM-based devices with a grid top electrode. The sample preparation as well as the experimental setup are described in detail in Ref. 1. The devices were illuminated for one hour with a halogen lamp (approximately 2.5 suns) in synthetic air at 298 K in order to ensure doping of the active layer.[5] They then remained under synthetic air for the duration of the experiment. An initial characterization was performed at room temperature, then the devices were cooled to 133 K. After performing the measurements at this temperature the samples were heated back to 303 K in increments of ten degrees. At each temperature the devices were allowed to equilibrate for approximately 30 minutes before characterization.

A. Electrical characterization

The complex permittivity $\underline{\varepsilon} = \varepsilon' + \hat{i}\varepsilon''$ is obtained from the complex impedance $\underline{Z_m} = Z' + \hat{i}Z''$, which is measured with an ac stimulus as small as $\hat{U} = 5$ mV to maintain the linearity of the current response. In order to compensate for parasitic series impedances, the samples were connected in a four terminal pair (4TP) configuration as described in Ref. 1. This configuration reduces the parasitic impedance induced by wires, cables, and connectors. However, it can only compensate to the point where the leads are connected to the electrodes. The series resistance inside the Ag fingers and the hole injecting layer remain uncompensated. The measured complex impedance $\underline{Z_m}$ hence needs correction for a temperature-dependent series resistance $R_s(T)$, yielding the corrected complex impedance $\underline{Z} = \underline{Z_m} - R_s(T)$. Undercompensation (i.e., R_s too small) results in the unphysical behavior of an ε' that rapidly approaches zero at high frequencies. In the case of overcompensation (i.e., R_s is too large), ε' shows an unphysical spike at high frequencies. Accurate compensation however yields an almost horizontal plateau at high frequencies with $\varepsilon' \geqslant 1$.

Indeed, we find a temperature-dependent parasitic component to the signal which can be approximated by $R_s(T) = 2.8\,\Omega + 2.9 \times 10^{-3}\,\frac{\Omega}{\mathrm{K}}(T - 303\,\mathrm{K})$, for which the measured impedance data is corrected.[22] Such a temperature dependance is typically found in metallic conductors.[23–26] This correction is sufficient to obtain a physically meaningful result for the real part of the dielectric function. However, parasitic out-of-phase components are not compensated for by this algorithm. Current-voltage (I-U) characterizations were performed with a Keithley 2400 Source Meter in 4TP mode.[27]

IV. RESULTS AND DISCUSSION

The complex impedance of an oxygen-doped inverted P3HT:PCBM bulk heterojunction solar cell was recorded at various temperatures and corrected for the temperature-dependent series resistance (Sec. III). Figure 2 displays the real part of the relative permittivity (ε') of the corrected data at various temperatures between 133 K and 303 K. The relative permittivity is calculated from the measured impedance spectra, assuming a surface area of the device of $A = 80\,\mathrm{mm}^2$ and a thickness of the active layer of $d = 200$ nm. The spectra can be divided into three sections: At low frequencies, ε' decreases modestly with increasing frequency. This regime is followed by an abrupt step at intermediate frequencies, which shifts towards higher frequencies with increasing temperature. At high frequencies, ε' becomes weakly dependent on frequency again, hence forming another plateau. The data points (dots) are shown together with best fits of the dispersive density of states model (lines) as defined by Eq. (1). From the fits, several important parameters, such as σ, N_{DOS}/U_{bi}, and f_0, can be extracted.

The fit parameter σ is a measure of how broad the transition between the low and the high frequency plateau of ε' is. Leaving this parameter as a variable in the fit procedure yields values which are very close to $\sigma = k_B T$ for the entire temperature range measured (compare Fig. S14). Fixing σ to $k_B T$ is interpreted as purely thermal broadening of the observed transition. Redoing the fits with $\sigma = k_B T$ hardly changes their quality (compare Fig. 2 to Fig. S3 and Fig. 3 to S4), even though one free fit parameter is removed from the

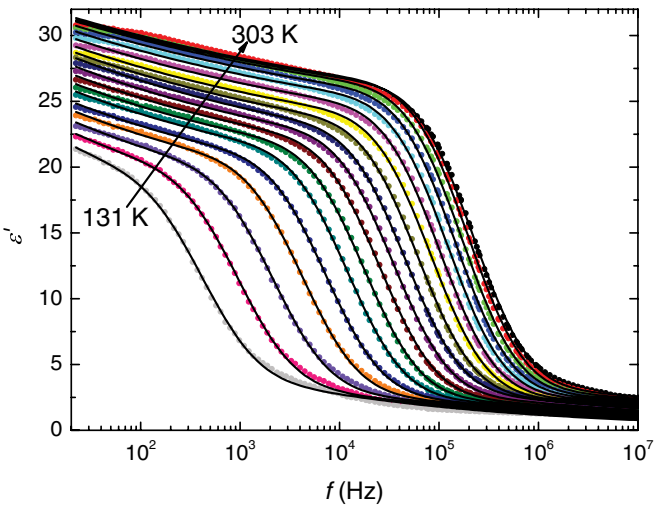

FIG. 2. (Color online) Real part of the relative permittivity (ε') of a doped-P3HT:PCBM-based device at various temperatures (dots). The lines represent best fits to the data using the formalism of the dispersive DOS model [Eq. (1) with $\sigma = k_B T$].

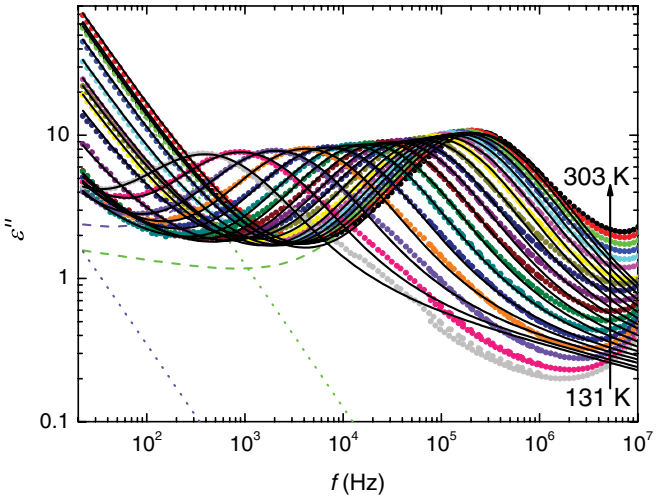

FIG. 3. (Color online) Imaginary part of the relative permittivity (ε'') of a doped-P3HT:PCBM-based device at various temperatures (dots). The solid lines represent the Kramers-Kronig transformed best fits to ε' as plotted in Fig. 2 and take the device's dc resistance (see Fig. 5) into account. The dashed green and purple lines are the uncorrected Kramers-Kronig transforms at 283 K and 153 K, respectively. The dotted lines represent the best correction for the device's dc resistance according to Eq. (6).

formalism. As a result the values extracted for this simplified fit procedure do not differ significantly from the initial ones. We hence only show the results for $\sigma = k_B T$ in the following and the comparison with the fits obtained by leaving σ a free fit parameter in the Supplemental Material.[22]

In Fig. 3 the imaginary part of the relative permittivity (ε'') is shown. The dispersive DOS model as presented in Eq. (1) is derived explicitly for the real part of the relative permittivity. However, ε' and ε'' are connected via the Kramers-Kronig relation.[28,29] The best fits to ε' can hence be transformed to obtain a description for the measured ε'' data. As we demonstrated in an earlier publication[1] there is also a second contribution to the experimental ε'' that needs to be taken into account, namely the device's small-signal dc resistance R_{dc}. This resistance yields an additive contribution to ε'' given by[1]

$$\varepsilon''_{dc} = \frac{d}{A\ \varepsilon_0\ 2\ \pi\ f} R_{dc}^{-1}. \tag{6}$$

R_{dc} can be extracted from the slope of the I-U curves in the dark around 0 V (Fig. 4), representing the leakage through the device. Hence this current is not associated with dielectric loss visible in the frequency dependance of ε'. R_{dc} values obtained from the I-U characteristics are shown as red circles in Fig. 5. Alternatively, R_{dc} can be obtained by performing a best correction of the numeric Kramers-Kronig transform according to Eq. (6). The results are shown in Fig. 5 as black dots. Both techniques yield virtually identical correction terms for the numeric Kramers-Kronig transform.

In Fig. 3 the theoretical curves obtained from a numerical Kramers-Kronig transformation including correction for the dc resistance are plotted as lines. Hence, they do not represent best fits to the ε'' data, but are the transformed fit curves compared to the experimental results. We note a discrepancy between the Kramers-Kronig transform and the experimental

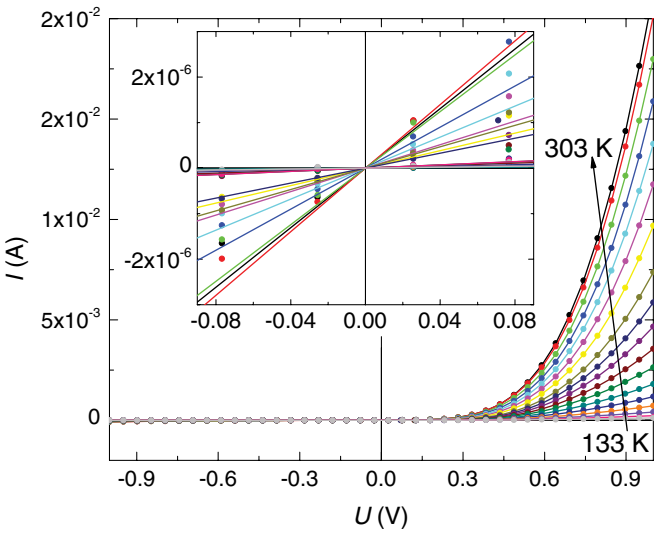

FIG. 4. (Color online) Current-voltage (I-U) characteristics of the sample at the temperatures for which the impedance spectra are taken. The inverse slope of the I-U curve around 0 V (see inset) is the device's small-signal dc resistance R_{dc}.

data at very high frequencies. We assign it to parasitic effects in the measurement data. While a temperature-dependent series resistance is sufficient to compensate these effects in ε' it does not take into account all parasitic contributions to ε''. However, the $1/f$ slope at low frequencies is assigned to the device's dc resistance and the relaxation peaks around f_0 are accurately reproduced by the Kramers-Kronig transformed data, both features backing the adequacy of the presented formalism. We interpret the excellent agreement between model and experiment as support for the applicability of our model over a wide temperature range.

Figure 6 shows the characteristic escape frequency f_0 obtained from fitting the dispersive DOS model to the real part of the relative permittivity measured at various temperatures.

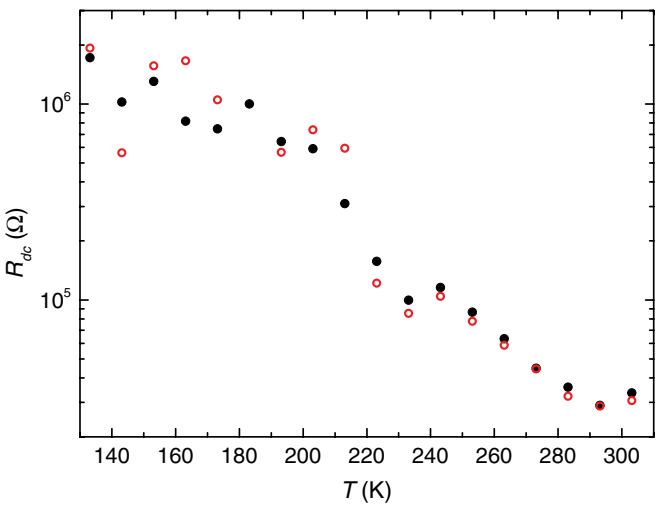

FIG. 5. (Color online) The dc device resistance R_{dc} obtained from a best correction of the numeric Kramers-Kronig transform data according to Eq. (6) (black dots). The inverse slope of the I-U curve around 0 V (inset of Fig. 4) is shown as red circles for comparison.

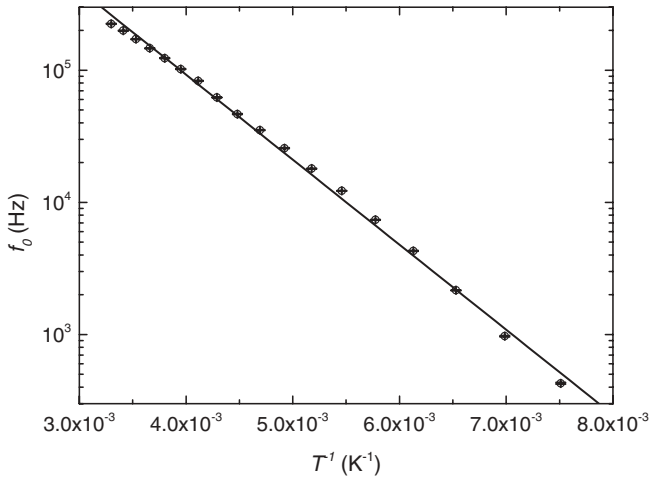

FIG. 6. Characteristic escape frequency f_0 (dots) as extracted from fitting Eq. (1) to ε' shown in Fig. 2 presented in an Arrhenius plot. The error bars represent the standard error of f_0. The line represents the best linear fit to the data.

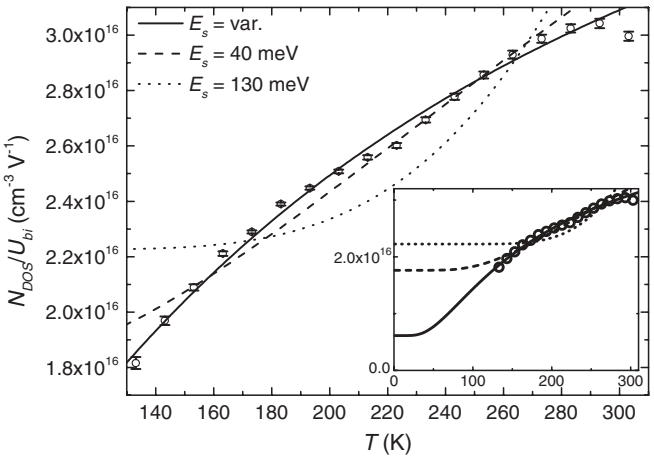

FIG. 7. Dopant concentration over built-in field (N_{DOS}/U_{bi}) obtained from fitting Eq. (1) to ε' (compare Fig. 2) (open circles) overlain with best fits of Eq. (7) to the data. The error bars represent the standard error of N_{DOS}/U_{bi}. The solid line represents a fit where E_s is a free fit parameter, resulting in $E_s = 14$ meV. Dotted line: Best fit with E_s fixed at 130 meV, the value found for the deep trap (Fig. 6). Dashed line: Best fit with E_s fixed at 40 meV, representing an upper limit for the depth of the shallow trap.

It has also been suggested to extract f_0 from the first derivative of ε'.[11] However, ε_g adds a contribution to the permittivity [Eq. (1)] which is not constant with frequency. The characteristic frequency f_0 hence deviates from the steepest slope of ε' or the maximum of $\partial\varepsilon'/\partial f$ (Fig. 2). For the same reason and the linearity of Kramers-Kronig transform f_0 is not identical to the frequency at which ε'' reaches its maximum value (Fig. 3).

The line in Fig. 6 represents the best fit of an Arrhenius equation [Eq. (2)] to the data. With this analysis over a wide temperature range we can support the previously assumed Arrhenius relation[1] between f_0 and the temperature T. Even more, the trap depth E_0 is calculated from the slope of the line in Fig. 6 as 130 meV and the predominant trap's attempt-to-escape frequency ν is 38 MHz. Both values are in good agreement with previously published data obtained for P3HT:PCBM by using various techniques.[30,31] Pure Arrhenius behavior is expected when the charge transport is only limited by a single type of deep trap. While assuming a dominating trap is not incompatible with our data we note a deviation of the extracted f_0 from the straight line in Fig. 6 which exceeds the statistical error. This is indicative of the presence of other, more shallow traps.

Another important device parameter that can be extracted from fitting Eq. (1) to ε' is N_{DOS}/U_{bi}, which is plotted in Fig. 7 as a function of temperature. We assume the built-in potential U_{bi} to be around 1 V[7] and independent of temperature; hence Fig. 7 suggests that the density of mobile charge carriers almost doubles between 133 K and 303 K from $1.8 \times 10^{16}\,\mathrm{cm}^{-3}$ to $3 \times 10^{16}\,\mathrm{cm}^{-3}$. After being illuminated in synthetic air (Sec. III) the active layer shows a significant concentration of dopants.

Assuming that the increase in available mobile charge carriers is due to thermal excitation from a trap to a transport level, N_{DOS}/U_{bi} vs temperature is expected to follow

$$\frac{N_{\mathrm{DOS}}}{U_{bi}} = \frac{N_d}{U_{bi}} + \frac{N_t}{U_{bi}} \exp\left(-\frac{E_s}{k_B T}\right), \qquad (7)$$

where N_d is the concentration of charge carriers introduced by doping, N_t is the concentration of charge carriers thermally promoted in the shallow trap level, and E_s is the depth of the shallow trap. The solid line in Fig. 7 represents the best fit of Eq. (7) to the data, where N_d/U_{bi}, N_t/U_{bi}, and E_s are free parameters. This yields a depth of the shallow traps of $E_s = 14$ meV. The dashed and dotted lines represent fits where E_s is fixed to 40 meV and 130 meV, respectively. Due to the limited temperature range investigated, the exact depth of the shallow trap cannot be determined and thus, the value of $E_s = 14$ meV can only be considered an estimation. The dashed line in Fig. 7 however suggests that the trap has to be shallower than 40 meV. Furthermore, this trap is clearly distinct from the trap with a depth of 130 meV (dotted line in Fig. 7). As illustrated here, the increase in the concentration of mobile charge carriers with temperature is not compatible with purely thermal excitation of trapped charge carriers over 130 meV.

However, a trap depth of 14 meV can explain this observation. We hence interpret this feature as the signature of shallow traps. These traps can easily be depopulated with the available thermal energy at room temperature (25 meV) and are hence able to take part in charge transport more easily than the deep traps. The characteristics of the shallow traps are not determined by directly fitting ε'. We can hence not assign an attempt-to-escape frequency or the broadening as we did for the deep traps.

After the assessment of N_{DOS}/U_{bi} and f_0 and with an estimate for ε_g at f_0, which can be obtained from Eq. (1), Eq. (5) allows for the determination of the mobility. It calculates the trap-limited mobility of holes drifting through the depletion zone in the active layer under the built-in potential. Figure 8 displays the mobility data obtained for various temperatures. It shows that the mobility increases with temperature, exceeding $10^{-3}\,\mathrm{cm}^2\,\mathrm{V}^{-1}\,\mathrm{s}^{-1}$ at 303 K. This number is in good agreement with mobility values obtained

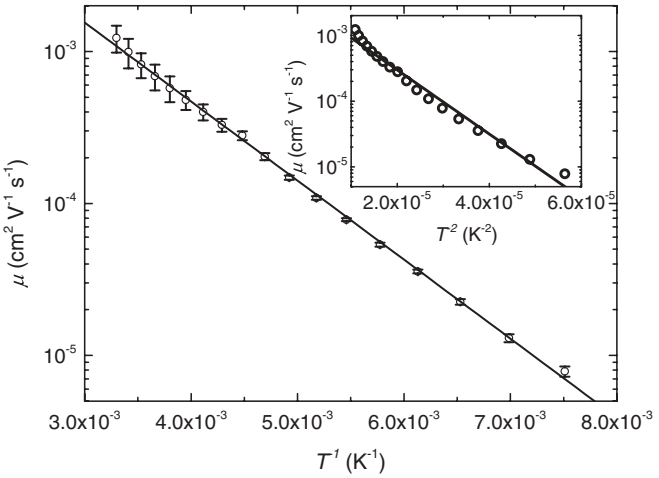

FIG. 8. Hole mobility at various temperatures as obtained from Eq. (5) in Arrhenius representation as well as vs T^{-2} (inset). The error bars represent the standard error of μ.

by transient techniques.[32] Interestingly, the mobility rather fits an Arrhenius model (i.e., T^{-1} law) as suggested by Craciun *et al.*[33] than obeying a T^{-2} law suggested by Bässler.[10]

V. CONCLUSION

We have demonstrated the value of dielectric spectroscopy for studying charge carrier trapping and transport characteristics in degraded organic solar cells. Analyzing impedance and *I-U* data obtained from oxygen-doped P3HT:PCBM devices over a wide temperature range allows for the determination of several important device parameters: The depth of the dominating trap is calculated as 130 meV. We also find the concentration of available mobile charge carriers to be dependent on temperature, essentially doubling between 133 K and 303 K. This observation is interpreted as the signature of a second, shallower trap level for holes, which is located approximately 14 meV above the transport level. Hence the depth of the shallow traps is on the order of the thermal energy at room temperature (25 meV). After exposure of the devices to synthetic air and white light of approximately 2.5 suns for one hour, the measured dopant concentration is of the order of 10^{16} cm^{-3}. From f_0 and the dopant concentration, the temperature-dependent mobility can be derived. At room temperature we determine the hole mobility as 10^{-3} cm^2 V^{-1} s^{-1}. The breadth of the transition between the low and the high frequency plateau seems to be consistent with $\sigma = k_B T$, hence being indicative of purely thermally broadened trap states. Experimental data over a temperature range from 133 K to 303 K supports the validity of our previously introduced model[1] for the impedance spectra of doped organic semiconductor devices. The successful application of our model introduces this technique as a way to determine the consequences of various degradation conditions and durations on the charge transport properties of organic semiconductor devices.

ACKNOWLEDGMENTS

The authors are indebted to Reinhard Schwödiauer for helpful discussions. Financial support by the German Ministry for Education and Research (BMBF) is acknowledged (projects "OPV Stability," FKZ 03SF0334A, and "EOS," FKZ 03X3516B).

*Present Address: Department of Physical Chemistry, University of Vienna, Währinger Straße 42, A-1090 Vienna, Austria; oskar.armbruster@univie.ac.at

†Present Address: Next Energy Technologies, Inc., 5385 Hollister Avenue, #115, Santa Barbara, California 93111, USA; christoph.lungenschmied@gmail.com

[1] O. Armbruster, C. Lungenschmied, and S. Bauer, Phys. Rev. B **84**, 085208 (2011).

[2] C. Lungenschmied, G. Dennler, H. Neugebauer, S. N. Sariciftci, M. Glatthaar, T. Meyer, and A. Meyer, Sol. Energy Mater. Sol. Cells **91**, 379 (2007).

[3] J. A. Hauch, P. Schilinsky, S. A. Choulis, R. Childers, M. Biele, and C. J. Brabec, Sol. Energy Mater. Sol. Cells **92**, 727 (2008).

[4] M. T. Lloyd, D. C. Olson, P. Lu, E. Fang, D. L. Moore, M. S. White, M. O. Reese, D. S. Ginley, and J. W. P. Hsu, J. Mater. Chem. **19**, 7638 (2009).

[5] A. Seemann, T. Sauermann, C. Lungenschmied, O. Armbruster, S. Bauer, H.-J. Egelhaaf, and J. Hauch, Sol. Energ. **85**, 1238 (2011).

[6] M. Jørgensen, K. Norrman, and F. C. Krebs, Sol. Energy Mater. Sol. Cells **92**, 686 (2008).

[7] G. Dennler, C. Lungenschmied, N. S. Sariciftci, R. Schwödiauer, S. Bauer, and H. Reiss, Appl. Phys. Lett. **87**, 163501 (2005).

[8] L. Lüer, H.-J. Egelhaaf, and D. Oelkrug, Opt. Mater. **9**, 454 (1998).

[9] H.-J. Egelhaaf, L. Lüer, D. Oelkrug, G. Winter, P. Haisch, and M. Hanack, Synth. Met. **84**, 897 (1997).

[10] H. Bässler, Phys. Status Solidi B **175**, 15 (1993).

[11] J. Parisi, V. Dyakonov, M. Pientka, I. Riedel, C. Deibel, C. J. Brabec, N. S. Sariciftci, and J. C. Hummelen, Z. Naturforsch. A **57**, 995 (2002).

[12] R. Kassing, Phys. Status Solidi A **28**, 107 (1975).

[13] P. P. Boix, G. Garcia-Belmonte, U. Muñecas, M. Neophytou, C. Waldauf, and R. Pacios, Appl. Phys. Lett. **95**, 233302 (2009).

[14] A. K. Jonscher, *Dielectric Relaxation in Solids* (Chelsea Dielectrics Press, 1983).

[15] I. D. Raistrick, D. R. Franceschetti, and J. R. Macdonald, in *Impedance Spectroscopy: Theory, Experiment, and Applications*, edited by E. Barsoukov and J. R. Macdonald (John Wiley & Sons, Inc., 2005), 2nd ed., Chap. 2.2.

[16] H. C. F. Martens, H. B. Brom, and P. W. M. Blom, Phys. Rev. B **60**, R8489 (1999).

[17] $p = 2M(2\pi f)^\gamma \sin\frac{\pi\gamma}{2} + M^2(2\pi f)^{2\gamma}\sin(\pi\gamma)$,
$q = 1 + 2M(2\pi f)^\gamma \cos\frac{\pi\gamma}{2} + M^2(2\pi f)^{2\gamma}\cos(\pi\gamma)$,
$r = [1 + M(2\pi f)^\gamma \cos\frac{\pi\gamma}{2}]^2 + M^2(2\pi f)^{2\gamma}\sin^2\frac{\pi\gamma}{2}$,
$s = \frac{M(2\pi f)^{1+\gamma}\sin\frac{\pi\gamma}{2}}{r}$,
$v = (2\pi f)[1 + M(2\pi f)^\gamma \cos\frac{\pi\gamma}{2}]$,
$u = \frac{v}{r}$,

$n = M(2\pi f)^{1+\gamma} \sin\frac{\pi\gamma}{2} - \frac{(2\pi f)^2}{2}$,
$g = -p(1 - \exp -s\cos u) - q\exp -s\sin u + v$,
$h = -q(1 - \exp -s\cos u) + p\exp -s\sin u - n$.

[18]M. Meier, S. Karg, and W. Riess, J. Appl. Phys. **82**, 1961 (1997).
[19]J. Scherbel, P. H. Nguyen, G. Paasch, W. Brütting, and M. Schwoerer, J. Appl. Phys. **83**, 5045 (1998).
[20]A. Assadi, C. Svensson, M. Willander, and O. Inganäs, J. Appl. Phys. **72**, 2900 (1992).
[21]D. M. Taylor and H. L. Gomes, J. Phys. D **28**, 2554 (1995).
[22]See Supplemental Material at http://link.aps.org/supplemental/10.1103/PhysRevB.86.235201 for data before and after correction. Figs. S1 and 2 illustrate the effect of the correction on the real part of the dielectric function, Figs. S2 and 3 on the imaginary part.
[23]J. Kim, J. Jung, D. Lee, and J. Joo, Synth. Met. **126**, 311 (2002).
[24]D. R. Lide, editor, *CRC Handbook of Chemistry and Physics*, 90th ed. (Taylor & Francis, 2009).
[25]D. J. Griffiths, *Introduction to Electrodynamics*, 3rd ed. (Prentice Hall, 1999).
[26]R. A. Serway, *Principles of Physics*, 2nd ed. (Brooks/Cole, 1997).
[27]*Agilent Impedance Measurement Handbook*, 4th ed. (Agilent Technologies, Inc., 2009).
[28]J. D. Jackson, *Classical Electrodynamics*, 3rd ed. (John Wiley & Sons, Inc., 1999).
[29]R. de L Kronig, J. Opt. Soc. Am. **12**, 547 (1926).
[30]J. Schafferhans, A. Baumann, C. Deibel, and V. Dyakonov, Appl. Phys. Lett. **93**, 093303 (2008).
[31]S. Neugebauer, J. Rauh, C. Deibel, and V. Dyakonov, Appl. Phys. Lett. **100**, 263304 (2012).
[32]A. Pivrikas, G. Juška, A. J. Mozer, M. Scharber, K. Arlauskas, N. S. Sariciftci, H. Stubb, and R. Österbacka, Phys. Rev. Lett. **94**, 176806 (2005).
[33]N. I. Craciun, J. Wildeman, and P. W. M. Blom, Phys. Rev. Lett. **100**, 056601 (2008).